Chemical inhibition of the auxin inactivation pathway uncovers the roles of metabolic turnover in auxin homeostasis

Kosuke Fukui[a] (ID), Kazushi Arai[b], Yuka Tanaka[b], Yuki Aoi[c], Vandna Kukshal[d] (ID), Joseph M. Jez[d] (ID), Martin F. Kubes[e] (ID), Richard Napier[e] (ID), Yunde Zhao[f] (ID), Hiroyuki Kasahara[g,h] (ID), and Ken-ichiro Hayashi[a,1] (ID)

The phytohormone auxin, indole-3-acetic acid (IAA), plays a prominent role in plant development. Auxin homeostasis is coordinately regulated by auxin synthesis, transport, and inactivation; however, the physiological contribution of auxin inactivation to auxin homeostasis has not been determined. The GH3 IAA–amino acid conjugating enzymes play a central role in auxin inactivation. Chemical inhibition of GH3 proteins *in planta* is challenging because the inhibition of these enzymes leads to IAA overaccumulation that rapidly induces *GH3* expression. Here, we report the characterization of a potent GH3 inhibitor, kakeimide, that selectively targets IAA-conjugating GH3 proteins. Chemical knockdown of the auxin inactivation pathway demonstrates that auxin turnover is very rapid (about 10 min) and indicates that both auxin biosynthesis and inactivation dynamically regulate auxin homeostasis.

auxin | plant hormone | chemical biology

Indole-3-acetic acid (IAA), the predominant natural auxin, is a master regulator for plant growth and development. Cellular IAA levels are strictly and dynamically regulated to ensure normal growth and development (1, 2). The homeostasis of IAA is thought to be coordinately modulated by three regulatory mechanisms: biosynthesis, transport, and inactivation (1–3). IAA is biosynthesized from tryptophan by two sequential enzymatic reactions catalyzed by the tryptophan–pyruvate aminotransferase TAA1 and the indole-3-pyruvate monooxygenase YUC in the indole-3-pyruvic acid (IPyA) pathway (4). In *Arabidopsis*, IAA is mainly inactivated by GH3–ILR1–DAO pathway that plays a central role in auxin homeostasis (5, 6) (*SI Appendix*, Fig. S1). In this pathway, IAA is initially conjugated with L-amino acids by the GRETCHEN HAGEN 3 (GH3) acyl amido synthetase family to form IAA–amino acid conjugates (7) (Fig. 1*A*). Two major conjugates, IAA–aspartate (IAA-Asp) and IAA–glutamate (IAA-Glu), function as temporal storage forms of IAA and these conjugates are reverted to IAA by ILR1/ILL amidohydrolases (5). DIOXYGENASE FOR AUXIN OXIDATION 1 (DAO1) irreversibly oxidizes IAA–amino acid conjugates into 2-oxoindoline-3-acetic acid (oxIAA)-Asp and oxIAA-Glu, which are further converted to oxIAA by ILR1 hydrolase (5, 8, 9). UDP-GLYCOSYLTRANSFERASE (UGT) family enzymes produce IAA–glucoside (IAA-Glc) (10, 11) and INDOLE-3-ACETATE *O*-METHYLTRANSFERASE 1 (IAMT1) enzyme converts IAA to IAA methyl ester. These two enzymes play a minor role in IAA inactivation in *Arabidopsis* plants (12–14).

In plants, the GH3 enzymes catalyze the conjugation of different amino acids to a variety of phytohormones and their precursors for either biosynthetic or inactivation purposes (15). For example, biosynthesis of the active jasmonate hormone Jasmonoyl–isoleucine (JA-Ile) requires the activity of AtGH3.11/JAR1 in *Arabidopsis* and its homologs in other plants (16, 17). Recently, the activity of AtGH3.12/PBS3 in *Arabidopsis* was implicated in the formation of a glutamyl conjugate of isochorismate that decomposes into the pathogen-response molecule salicylic acid (SA) (18). The roles of other GH3 homologs, such as AtGH3.7, in Brassica also suggests similar functions in SA synthesis (6). In contrast, the formation of IAA conjugates, especially IAA-Asp and IAA-Glu, by multiple GH3 proteins has long been associated with auxin homeostasis (1, 7, 19). In *Arabidopsis*, eight GH3 proteins function as auxin-inactivating enzymes that conjugate IAA with either Asp (AtGH3.1-AtGH3.6) or Glu (AtGH3.9 and AtGH3.17) to attenuate auxin responses (7, 20, 21). Moreover, some isoforms (*AtGH3.1-AtGH3.6*) are auxin-inducible, whereas others are auxin-nonresponsive (*AtGH3.9* and *AtGH3.17*) (20, 21). These expression profiles suggest that *AtGH3.9* and *AtGH3.17* maintain basal IAA inactivation and auxin-inducible *GH3s* may modulate temporal shifts in local IAA levels. Recently, AtGH3.15 was shown to selectively convert indole-3-butyric acid (IBA) to IBA-Gln (22). The activity of this GH3 protein would affect IAA homeostasis, as IBA is a precursor of IAA produced by β-oxidation in the peroxisome.

Significance

The phytohormone auxin, indole-3-acetic acid (IAA), is a key regulator in plant growth. The intracellular auxin level is precisely regulated in response to developmental and environmental cues. Auxin inactivation plays an important role in auxin homeostasis. Auxin is predominantly inactivated by conjugating it to amino acids—reactions catalyzed by the GH3 enzymes. Auxin rapidly induces the expression of auxin-inactivating *GH3* family genes, thus forming a negative feedback loop for maintaining IAA levels. Using kakeimide, a selective inhibitor for auxin-inactivating GH3 enzymes, we demonstrate that auxin homeostasis is dynamically maintained by the rapid turnover of IAA (about 10 min) and that the GH3 pathway plays a central role in auxin inactivation in various plant species.
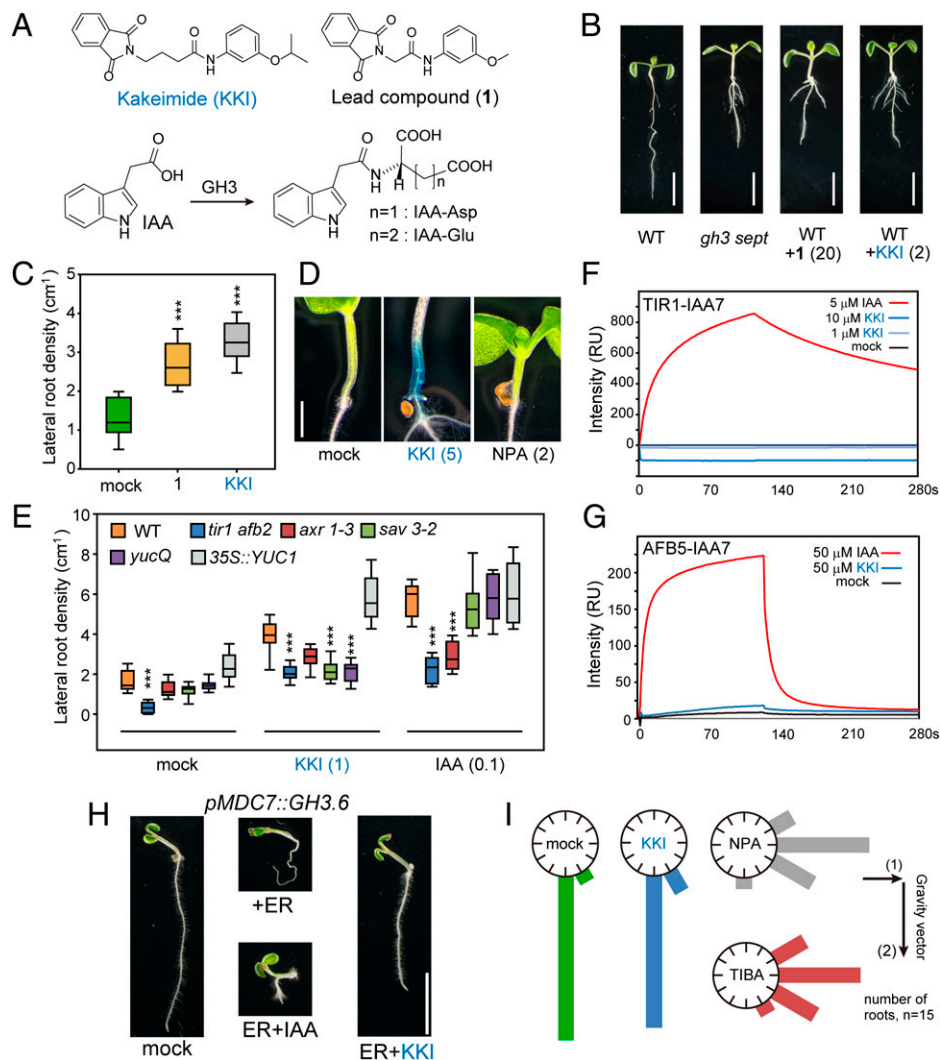
Fig. 1. KKI showed auxin-like activity by inhibiting endogenous IAA catabolism. (*A*) Structure of IAA, IAA-Asp, IAA-Glu, active lead compound **1** and KKI. (*B*) Phenotype of 7-d-old *gh3 septuple* mutant and WT plants treated with chemicals. The values in parentheses represents the concentration of chemicals (micromolar). (Scale bar: 5 mm.) (*C*) Effects of KKI on lateral root formation. WT seedlings (4-d-old) were treated with 1 μM chemicals for another 3 d (***$P <$ 0.001, Tukey's honestly significant difference [HSD] test, $n = 21$). (*D*) Effects of KKI on *DR5::GUS* reporter expression and adventitious root formation. *DR5::GUS* reporter lines were grown with 5 μM KKI or 2 μM NPA for 7 d. (Scale bar: 1 mm.) (*E*) Effects of KKI on lateral root formation in auxin-signaling mutants (*tir1afb2* and *axr1-3*) and biosynthetic mutants (*sav3-2*, *yucQ*, and *35S::YUC1*). The *sav3-2* mutant and *yucQ* mutant were cotreated with 1 μM yucasinDF or 1 μM kynurenine, respectively. The 4-d-old seedlings were incubated with KKI for another 3 d. The lateral root number and root length were measured. Asterisks indicate a statistically significant difference relative to WT (***$P < 0.001$, Tukey's HSD test, $n = 18$). (*F* and *G*) SPR analysis of the auxin-induced interaction between TIR1/AFB receptors and IAA7 degron peptide. The sensorgram shows the effect of IAA (red) and KKI (blue) on TIR1–IAA7 peptide association and dissociation (*F*) and AFB5–IAA7 peptide association and dissociation (*G*). (*H*) Effects of KKI on auxin-deficient phenotype in estradiol-inducible *GH3.6*-overexpressing line. The *GH3.6ox* line was grown with or without 5 μM estradiol (ER) and 5 μM KKI for 4 d. (Scale bar: 10 mm.) (*I*) Effects of KKI on root gravitropic response. Six-day-old seedlings were transferred onto GM agar plates containing 2 μM KKI, 2 μM NPA, or 5 μM TIBA and vertically grown for 2 h. The plate was then rotated at 90° angle against vertical direction and then cultured for 18 h. The arrows indicate the gravity vector before (1) and after (2) the commencement of gravistimulation. The angles were grouped into 30° classes and plotted as circular histograms ($n = 15$).

Recent genetic approaches to GH3 protein function indicate that *GH3* genes show redundancy in IAA inactivation, although some GH3s play a crucial role in particular developmental events and environmental responses (23, 24). *AtGH3.17* regulates IAA homeostasis in hypocotyls in response to shade and high temperature (25). *AtGH3.9* plays a role in IAA catabolism to regulate fertility in *Arabidopsis* (23, 24). Multiple *GH3* mutants generated using CRISPR-Cas9 gene editing technology demonstrated that three GH3 proteins, GH3.5, GH3.6, and GH3.17, mainly contribute to IAA inactivation (23). Furthermore, *gh3-1 2 3 4 5 6 9 17 octuple* mutants exhibit severe auxin overaccumulation phenotypes, such as short primary roots and many lateral roots (23, 24). Although these genetic approaches provide insight into the physiological role of each *GH3* gene, it is challenging to assess the spatiotemporal role of auxin inactivation in auxin homeostasis using

genetic approaches. For example, in *gh3 octuple* null mutants, auxin homeostasis can be redundantly modulated by biosynthesis and transport (23).

The spatiotemporal analysis of auxin homeostasis can be precisely controlled by chemical modulators, such as inhibitors of auxin biosynthesis and inactivation (26). Some IAA biosynthesis inhibitors have been developed. ʟ-kynurenine and pyruvamine competitively inhibit TAA1 (26). The YUC monooxygenase inhibitors PPBo and yucasin DF also block IAA production and are used as molecular probes of auxin biosynthesis (26, 27). Adenosine-5-[2-(1H-indol-3-yl)ethyl]phosphate (AEIP) was the first competitive inhibitor of the IAA-conjugating GH3 proteins (28). AEIP is an analog of reaction intermediate of IAA-adenosine monophosphate ester and shows in vitro activity against auxin-conjugating GH3s in the micromolar range. Similarly, the molecule

jarin-1 selectively inhibits the GH3 protein (AtGH3.11/JAR1) responsible for conjugating isoleucine to jasmonic acid (JA) to form JA-Ile (29). Multiple GH3 proteins are encoded by early auxin-inducible genes and inhibition of IAA-conjugating GH3s leads to accumulation of IAA, which rapidly induces expression of several GH3s *in planta* (30). Thus, the design of effective inhibitors targeting the auxin-conjugating GH3s *in planta* can be highly challenging.

Here we report the characterization of kakeimide (KKI), which specifically inhibits IAA-conjugating GH3 enzymes at subnanomolar concentrations in vitro. KKI induced high-auxin phenotypes, including primary root inhibition and lateral root promotion, and phenocopied the *gh3 octuple* mutant. By using KKI and metabolite analysis, we demonstrate that the turnover time of endogenous IAA is estimated to be about 10 min in *Arabidopsis*, indicating that modification by GH3 enzymes plays a crucial role in the dynamics of auxin homeostasis. KKI treatments led to high-auxin phenotypes in diverse land plants including rice and moss. Thus, KKI is a promising chemical tool for dissecting auxin homeostasis in diverse plants.

Results

KKI Caused Auxin Overaccumulation Phenotypes by Inhibiting Endogenous IAA Catabolism.
To find a lead compound that inhibits IAA-conjugating GH3 enzymes in vivo, we performed a phenotype-based screen using *Arabidopsis GH3.6*-overexpressing plants (*GH3.6ox*). *Arabidopsis GH3.6*-overexpressing plants showed the typical auxin-deficient phenotypes such as no root hairs and few lateral roots (*SI Appendix*, Fig. S2). From a synthetic chemical library (9,600 compounds), we identified active compounds that restored root hair defects in auxin-deficient *GH3.6ox* roots. Active compounds were further evaluated according to the effects on the high-auxin phenotypes in IAA-overproducing *YUC6* overexpression (*YUC6ox*) plants. GH3 inhibitors would reduce IAA inactivation and result in similar extreme high-auxin phenotypes as *YUC6ox* plants. From the results, compound **1** (CAS registry number: 139088-71-4) was selected as a lead GH3 inhibitor from the initial evaluation (*SI Appendix*, Fig. S2). We optimized the structures of lead compound **1** based on the crystal structure of GH3 enzymes (22, 31) and designated one of the most potent inhibitors as KKI (Fig. 1*A*) (5).

To investigate the biological activity of KKI in vivo, we examined the effects of KKI on growth and development of *Arabidopsis* plants. Wild-type (WT) seedlings grown with 2 μM KKI displayed high-auxin phenotypes such as short primary roots and more lateral roots (Fig. 1 *B* and *C* and *SI Appendix*, Fig. S3). The phenotypes were similar to those of the *gh3-1, 2, 3, 4, 5, 6, 17* septuple (*gh3-sept*) mutants (23) (Fig. 1*B* and *SI Appendix*, Fig. S4). Furthermore, KKI at 5 μM induced the expression of the auxin-responsive *DR5::GUS* reporter gene and promoted adventitious root formation in *Arabidopsis* hypocotyls (Fig. 1*D*) (32).

Next, we examined the effects of KKI on multiple auxin signaling and biosynthesis mutants (Fig. 1*E*). The *tir1-1 afb2-1* double mutants have defects in two auxin receptors (33) and the *axr1-3* has a mutation in a subunit of the RUB1-activating enzyme that is a regulatory component of the SCF$^{TIR1/AFB}$ coreceptor complex (34). The auxin signaling mutants exhibited resistance to auxin due to impaired auxin signaling. The auxin biosynthesis mutants *sav3-2/taa1* and *yuc Q* (*yuc 3 5 7 8 9* quintuple) lead to loss of function in the IPyA pathway (35, 36).

In our assays, the auxin signaling mutants *tir1-1 afb2-1* and *axr1-3* showed resistance to both IAA and KKI in lateral root

formation (Fig. 1*E*). Lateral roots of *taa1/sav3-2* and *yuc Q* mutants were induced by IAA to a similar extent as WT plants. In contrast, KKI failed to promote lateral root formation in the *sav3-2* and *yuc Q* mutants (Fig. 1*E*). Consistent with the lateral response to KKI in IAA biosynthesis mutants, the IAA biosynthesis inhibitor yucasin DF (27) reversed the high-auxin phenotypes of *gh3-sept* mutants and KKI-treated WT plants (*SI Appendix*, Fig. S5). These results suggest that KKI does not act as an active auxin that directly modulates SCF$^{TIR1/AFB}$ auxin signaling and that endogenous IAA is essential for KKI-induced high-auxin phenotypes. These findings were supported by biochemical assays using surface plasmon resonance (SPR) analysis (37). In this assay, IAA promotes interaction between AtTIR1/AFB auxin receptor and the AtIAA7 Aux/IAA degron peptide (Fig. 1 *F* and *G*). KKI did not affect the association and dissociation between either the AtTIR1–IAA7 peptide or AtAFB5–IAA7, which indicates that KKI does not function as an agonist of auxin coreceptors. Some structurally divergent compounds have been reported to show auxin-like activity, and some are found to act as prohormones that are converted metabolically to active synthetic auxin molecules (26). Thus, we examined auxinic activity of possible metabolites of KKI. The likely hydrolysis products of KKI did not show any auxinic activity at the same concentration of KKI (*SI Appendix*, Fig. S6), suggesting that the metabolized products of KKI do not act as synthetic auxins.

We next assessed the effects of KKI on cellular IAA levels in *Arabidopsis* roots. IAA at 0.05 μM promoted lateral root formation in WT roots. Two micromolar KKI slightly induced lateral root formation. Cotreatment with IAA and KKI dramatically promoted lateral root formation (*SI Appendix*, Fig. S7*A*). Consistently, the IAA-overproducing *YUC6*-overexpressing line *pMDC7::YUC6* showed higher sensitivity to KKI than WT regarding lateral root formation (*SI Appendix*, Fig. S7*B*). Additionally, the endogenous IAA level in KKI-treated WT seedlings was twofold higher than in mock-treated plants (*SI Appendix*, Fig. S7*C*). In another IAA overproducer, a *35S::YUC1*-overexpressing line, the IAA level was threefold higher than in the mock-treated line (*SI Appendix*, Fig. S7*C*). This evidence suggested that KKI increases endogenous IAA levels by inhibiting IAA inactivation pathways.

AtGH3.6-overexpressing plants showed severe auxin-deficient phenotypes, such as stunted root growth (Fig. 1*H*). KKI rescued the auxin-deficient phenotype of these *AtGH3.6* overexpressing plants, which suggests that KKI targets auxin-conjugating GH3 enzymes (Fig. 1*H*). The inhibition of root gravitropism is a characteristic of auxin transport inhibitors, such as *N*-naphthylphthalamic acid (NPA) and 2,3,5-triiodobenzoic acid (TIBA) (26, 38). These auxin transport inhibitors also repress the lateral root formation (39). KKI did not inhibit root gravitropism (Fig. 1*I* and *SI Appendix*, Fig. S8*A*) but promoted lateral and adventitious root formation (Fig. 1 *B* and *D* and *SI Appendix*, Fig. S7*A*). Furthermore, auxin transport inhibitors induced DR5 reporter expression near the quiescent center where IAA is biosynthesized, whereas KKI strongly induced DR5 reporter expression in columella and lateral root cap cells (*SI Appendix*, Fig. S8 *B* and *C*). These results indicate that KKI does not inhibit auxin efflux transport.

KKI Specifically Inhibits Auxin-Conjugating GH3 Enzymes In Vivo.
To investigate the selectivity of KKI on auxin inactivation pathways in vivo, we assessed the phenotypic effects of KKI on overexpressing lines of various types of auxin-modifying enzymes. UGT84B1 catalyzes the formation of IAA-β-D-glucoside and IAMT1 converts IAA to IAA methyl ester

(12, 13). We generated *Arabidopsis UGT84B1*, *IAMT1*, and *GH3* (*AtGH3.2*, *AtGH3.3*, *AtGH3.5*, *AtGH3.6*, *AtGH3.17*, and *OsGH3-8*)–overexpressing lines (Fig. 2 *A–C*). Exogenous IAA promoted lateral root formation in WT roots. Overexpression of the IAA-modifying enzymes *AtGH3.6*, *AtGH3.17*, *OsGH3-8*, *IAMT1*, and *UGT84B1* repressed IAA-induced lateral root formation (Fig. 2 *A–C*), which indicates that excess IAA is readily inactivated by IAA-modifying enzymes in these overexpression lines. Cotreatment with KKI and IAA greatly enhanced lateral root formation in the GH3-overexpression lines but failed to promote lateral root formation in the *IAMT1*- and *UGT84B1*-overexpressing lines (Fig. 2 *B* and *C*). These results demonstrate that KKI specifically inhibits the GH3-mediated IAA inactivation pathway *in planta*. Additionally, we examined the effects of KKI on JA-Ile formation by AtGH3.11/JAR1. Exogenously applied JA and JA methyl ester are converted to JA-Ile by AtGH3.11/JAR1 and then JA-Ile activates JA signaling via SCF^COI1 JA-Ile receptors (16, 17). JA induced the degradation of JAZ1-GUS repressor fusion protein via SCF^COI1 signaling and also activated JA-inducible *pJAZ2::GUS* expression (29). KKI did not affect JA-induced responses in these two reporter lines (Fig. 2*D* and *SI Appendix*, Fig. S9*A*). Exogenous JA induces anthocyanin accumulation in *Arabidopsis* shoots via the COI-1 JA-Ile receptor (*SI Appendix*, Fig. S9*B*) (40). The *coi-1* mutant was insensitive to JA-induced accumulation of anthocyanin. Consistent with JAZ-reporter assays, KKI did not affect JA-induced accumulation of anthocyanin. These results indicate that KKI does not inhibit the formation of JA-Ile by AtGH3.11/JAR1 in planta.

Inhibitory Activities of KKI on Recombinant GH3 Enzymes In Vitro. To assess the mode of inhibition of KKI on GH3 enzymes, we conducted in vitro enzyme assays with recombinant

GH3 proteins: *Arabidopsis* AtGH3.3, AtGH3.5, AtGH3.6, and AtGH3.17 (7, 41). We initially examined the inhibitory effects of KKI on AtGH3.6 and AtGH3.17 as representatives of IAA-conjugating GH3s. AtGH3.17 and AtGH3.6 synthesize IAA-Glu and IAA-Asp, respectively, from IAA, ATP, and the corresponding amino acids, L-Glu and L-Asp. The GH3 conjugation reaction requires a ping-pong bi bi kinetic mechanism (41). In this sequence, a GH3 initially binds to ATP, and subsequently the GH3•ATP complex reacts with IAA to form IAA–AMP, an acylated reaction intermediate. In the next step, GH3 conjugates IAA–AMP and an amino acid to form the IAA–amino acid conjugate as the final product. AtGH3.17 enzyme produced IAA-Glu (Fig. 3 *A* and *C*), and KKI inhibited the formation of IAA-Glu by AtGH3.17 (Fig. 3*B*). A double-reciprocal plot of AtGH3.17 indicated that KKI competitively inhibited GH3 activity toward IAA as the substrate. A similar analysis showed that the inhibition mode of KKI was uncompetitive versus ATP and noncompetitive for the amino acid substrate (Fig. 3 *D–G*). Furthermore, KKI showed the same modes of inhibition for IAA and ATP with AtGH3.6, as shown in *SI Appendix*, Fig. S10. KKI showed very potent inhibitory activity on AtGH3.17 with a K_i^{IAA} of 340 pM (Fig. 3*G*) and with subnanomolar K_i^{IAA} with other auxin-conjugating GH3s, AtGH3.3, AtGH3.5, and AtGH3.6 (Fig. 3*H*). This potent inhibitory activity most likely overcomes the IAA-inducible GH3 activity *in planta*.

The inhibition data, along with the kinetic mechanism of the GH3, indicate that KKI binds to the IAA binding site of the GH3•ATP complex to form a ternary complex (32, 42). Thus, the GH3•ATP•KKI complex would inhibit the synthesis of IAA–amino acid conjugates. To further substantiate the inhibitory mechanism of KKI, we examined the inhibitory effects of KKI on AtGH3.15, which prefers IBA as a substrate
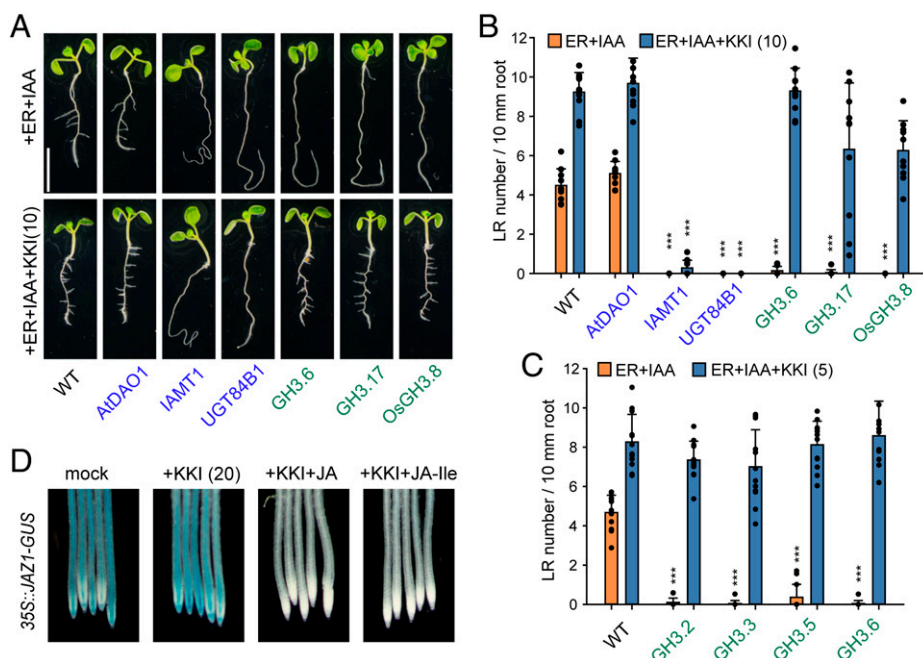

Fig. 2. KKI specifically inhibits auxin-conjugating GH3 enzymes. (*A–C*) Effects of KKI on the lateral root formation in IAA catabolic enzymes overexpressing lines. WT and estradiol-inducible *GH3*-, *IAMT1*-, *UGT84B1*-, and *AtDAO1*-overexpressing lines (4-d-old) were cultured for 3 d on a GM plate containing 5 μM estradiol (ER) and 0.05 μM IAA with or without KKI. (*A*) Representative picture of plants after 3-d incubation with or without 10 μM KKI. (Scale bar: 10 mm.) (*B* and *C*) The lateral root number and root length were measured. The orange bar represents lateral root density cotreated with 5 μM ER and 0.05 μM IAA. The blue bar represents lateral root density cotreated with 5 μM ER, 0.05 μM IAA and KKI (*B*: 10 μM, *C*: 5 μM). Asterisks indicate a statistically significant difference relative to WT (***$P < 0.001$, Tukey's HSD test; *B*, $n = 12$; *C*, $n = 10$). (*D*) KKI did not affect the conjugation of JA with Ile by AtGH3.11/JAR1 *in planta*. The JAZ1-GUS fusion protein–expressing line (7-d-old) was incubated with 20 μM KKI for 1 h then treated with either JA or JA-Ile for an additional 30 min. The values in parentheses represents the concentration of chemicals (micromolar).
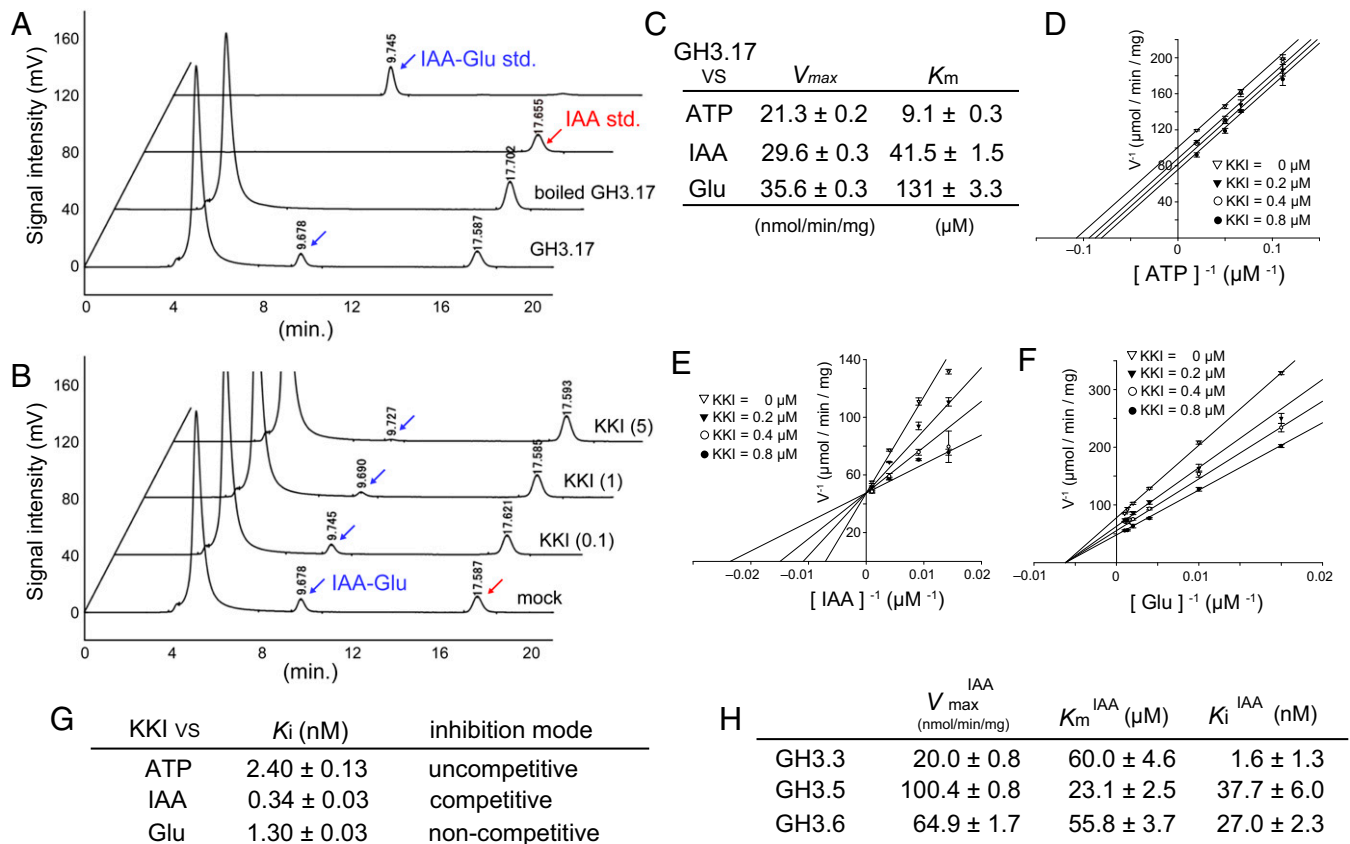
Fig. 3. Kinetic analysis for the inhibitory effect of KKI against GH3 enzyme. (*A*) HPLC chromatograms of AtGH3.17 reaction mixture. The peaks (retention times = 9.7 min and 17.6 min) indicate IAA-Glu and IAA, respectively. Boiled AtGH3.17 did not produce IAA-Glu. (*B*) KKI inhibited AtGH3.17 activity in a dose-dependent manner. KKI decreased the production of IAA-Glu (at 9.7 min). The values in parentheses represent the concentration of chemicals (micromolar). (*C*) The maximum velocity (V_{max}) and Michaelis constant (K_m) of AtGH3.17 for ATP, IAA, and Glu substrates. (*D*–*F*) A double-reciprocal plot of AtGH3.17 activity in the presence of KKI. (*D*) KKI uncompetitively inhibits AtGH3.17 toward ATP. (*E*) KKI competitively inhibits AtGH3.17 toward IAA. (*F*) KKI noncompetitively inhibits AtGH3.17 toward Glu. (*G*) The inhibition constant (K_i) and mode of inhibition of AtGH3.17. (*H*) The kinetic parameters (V_{max}, K_m, and K_i) of AtGH3.3, AtGH3.5, and AtGH3.6 toward IAA. Error bars in *D*–*F* are SE ($n = 3$). Average values ± SE ($n = 3$) are shown in *G* and *H*.

over IAA and forms IBA-Gln from IBA, ATP, and Gln (22). Consistent with our inhibition model, KKI did not inhibit AtGH3.15 (*SI Appendix*, Fig. S11), which supports the *in planta* data that KKI selectively targets IAA-conjugating GH3s. We next examined KKI binding to the GH3s by molecular docking (*SI Appendix*, Fig. S12). Previous X-ray crystal structures revealed the key features that tailor the substrate binding site of the GH3s and indicate that the IAA binding site of AtGH3.5 is different from the IBA binding cavity of AtGH3.15 (17, 22, 32). Docking results suggest that KKI could fit well within the IAA binding site of VvGH3.1, AtGH3.5, and OsGH3-8 but that KKI would not fit in the IBA binding site of AtGH3.15. This would account for the observed selectivity of KKI for IAA-conjugating GH3s.

KKI Treatments Led to Rapid Accumulations of Endogenous IAA within 10 min In Planta. The *gh3-octuple* mutants showed extreme high-auxin phenotypes (23); however, the steady state of IAA homeostasis could not be estimated using the *gh3* mutant analysis because IAA biosynthesis would be decreased and IAA efflux transport would be enhanced under the high level of IAA in this mutant. In contrast, specific chemical inhibition of IAA-conjugating GH3s enables the spatiotemporal modulation of IAA homeostasis in WT plants. To visualize the dynamic change of cellular IAA level in vivo, we examine the effects of KKI on the auxin-dependent degradation of DII-VENUS fusion reporter protein (Fig. 4 *A* and *B*) (44). The

nuclear-localized DII-VENUS proteins are rapidly decomposed after IAA application, within 10 min as previously reported (43). As shown in Fig. 4*B*, KKI initiates the degradation of DII-VENUS proteins within 10 min and the DII-VENUS signal is completely lost after 40 min. These results suggest that KKI instantly blocked IAA inactivation by GH3, leading rapidly to increased endogenous IAA levels. We next measured endogenous IAA levels by liquid chromatography tandem mass spectrometry (LC-MS/MS) analysis in the root (Fig. 4*C*). After treatment with KKI for 10 min, the endogenous IAA level was twofold higher than mock treatment and IAA levels continued to increase with incubation time (Fig. 4*C*). These results demonstrated the experimentally estimated turnover time of endogenous IAA in normal plants to be about 10 min, which is a pivotal parameter in auxin homeostasis. Consistent with the impact of KKI on IAA levels, KKI up-regulated the expression of typical auxin-responsive genes *AtGH3.3* and *IAA19* within 30 min, just as done by IAA (Fig. 4*D*). Both KKI and IAA transcriptionally down-regulated the auxin biosynthesis gene *YUC6* after 60 min of treatment due to negative feedback from elevated auxin levels.

KKI Induced Auxin Responses in Various Plants by Inhibiting IAA Inactivation. To assess the physiological role of IAA homeostasis mediated by GH3 in different plant species, we initially investigated the GH3 pathway in *Arabidopsis* plants overexpressing the rice *OsGH3-8* enzyme. KKI blocked IAA inactivation by

5 of 10

rice *OsGH3-8* (Fig. 2 *A* and *B*) in *Arabidopsis* seedlings. Additionally, KKI inhibited recombinant OsGH3-8 enzyme activity in vitro (Fig. 5*A*). This implies that KKI could also modulate in vivo IAA inactivation by GH3 pathways in rice. To reveal the physiological role of GH3 pathways, we examined the phenotypic effects of KKI on rice seedlings (Fig. 5*B* and *SI Appendix,* Fig. S13). In rice roots, both IAA and KKI suppressed primary root elongation, and KKI enhanced the inhibition of root elongation by IAA. In the aerial part of rice seedlings, IAA and KKI promoted mesocotyl elongation. Consistent with this phenotypic analysis, KKI induced the expression of auxin-responsive *OsIAA1* and *OsGH3-8* genes in roots to the same extent as IAA (Fig. 5*C*), indicating that KKI increased IAA level by inhibiting GH3 enzymes in rice.

We next performed the phenotypic analysis on four higher plants, *Nicotiana tabacum* (tobacco, Solanaceae), *Vigna radiate* (mung bean, Fabaceae), *Lactuca sativa* (lettuce, Asteraceae), and *Daucus carota* (carrot, Apiaceae), and the moss *Physcomitrium patens* (Fig. 6). In a tobacco auxin-responsive *PS-IAA4/5::GUS* reporter line, KKI induced auxin-responsive GUS reporter expression (Fig. 6*A*). In the root phenotypes of all four vascular plants, KKI inhibited primary root growth and induced lateral root formation, suggesting IAA would be primarily inactivated by the GH3 pathway in these vascular plants

(Fig. 6 *A–D*). In the moss *P. patens*, KKI strongly induced auxin-responsive *GH3::GUS* reporter expression in the leafy gametophore (Fig. 6*E*). Intriguingly, KKI perturbed leaf formation and triggered the ectopic formation of new primordia of leafy-like tissue (Fig. 6 *F* and *G* and *SI Appendix,* Fig. S14). This ectopic formation of leafy-like primordia has not been induced by exogenous IAA application, indicating that GH3s play a role in the auxin gradient formation leading to the leafy-like primordia formation in the moss *P. patens*.

Discussion

The GH3-mediated IAA inactivation pathway plays an important role in auxin homeostasis. We performed a phenotype-based screen using a *GH3.6*-overexpressing line of *Arabidopsis* to find GH3 inhibitors, and we conducted structural optimization of a lead compound. Consequently, we found KKI to be a potent and specific inhibitor for IAA-conjugating GH3s (5). We herein demonstrated the characterization of KKI and revealed the physiological role of the auxin-inactivating GH3 pathway. KKI blocked IAA inactivation *in planta*, resulting in a high-auxin phenotype (Figs. 1 and 2). Kinetic analysis (Fig. 3) revealed that KKI competitively binds to the IAA binding site in the GH3•ATP [E•S] complex to form an GH3•ATP•KKI
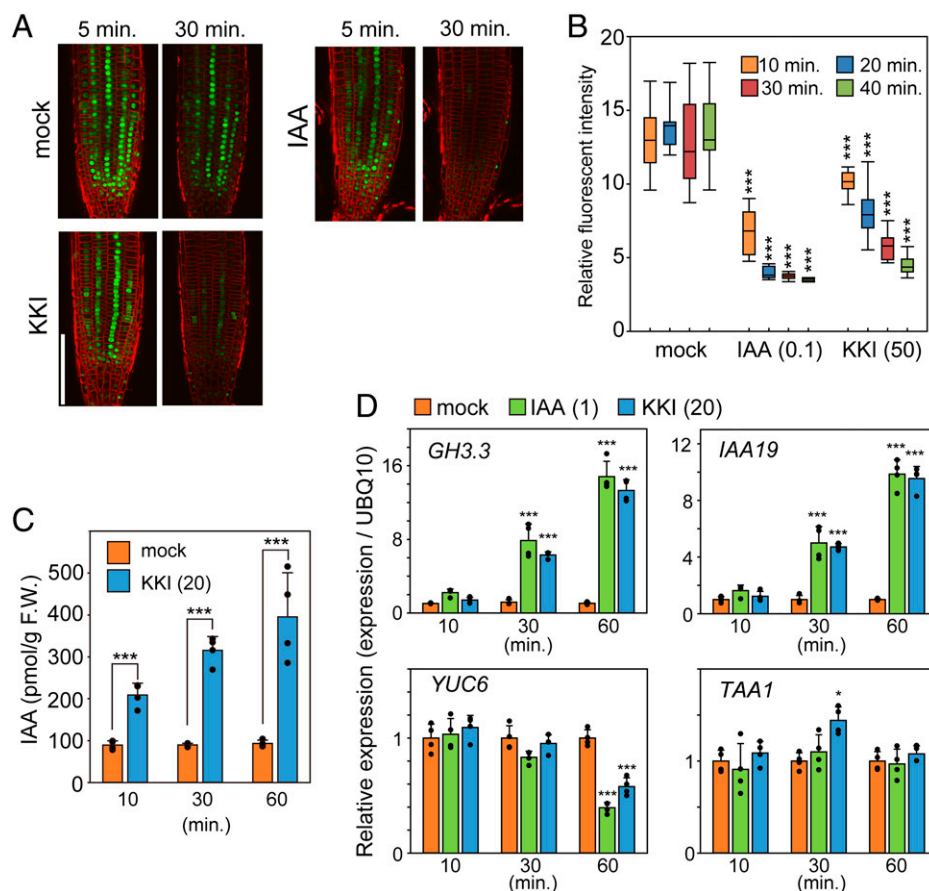

Fig. 4. KKI rapidly accumulates endogenous IAA. (*A*) Effects of KKI on the auxin-inducible degradation of DII-VENUS fusion proteins. The DII-VENUS fusion protein was monitored by confocal microscopy at regular intervals after 0.1 μM IAA or 50 μM KKI treatment. KKI promoted the degradation of DII-VENUS protein same as IAA. (Scale bar: 50 μm.) (*B*) Quantitative analysis of fluorescence intensity of DII-VENUS protein. The fluorescent intensity of root tips (*n* = 10) was measured with ImageJ software in each treatment for indicated minutes. The values in parentheses represent the concentration of chemicals (micromolar). (*C*) Endogenous IAA levels of WT plants after KKI treatment. Ten-day-old WT seedlings were transferred to liquid GM culture containing 20 μM of KKI. IAA content in roots was measured by LC-MS/MS (*n* = 4). Error bars are SD. (*D*) Effects of KKI on auxin-related gene expression. Relative gene expression levels were quantified with real-time PCR (*n* = 4). All data were standardized according to the expression levels of *UBQ10*. Eight-day-old WT plants were treated with the KKI for 10 to 60 min. (*C* and *D*) Asterisks indicate a statistically significant difference relative to mock treatment (*$P < 0.05$, ***$P < 0.001$, Tukey's HSD test, *n* = 4).
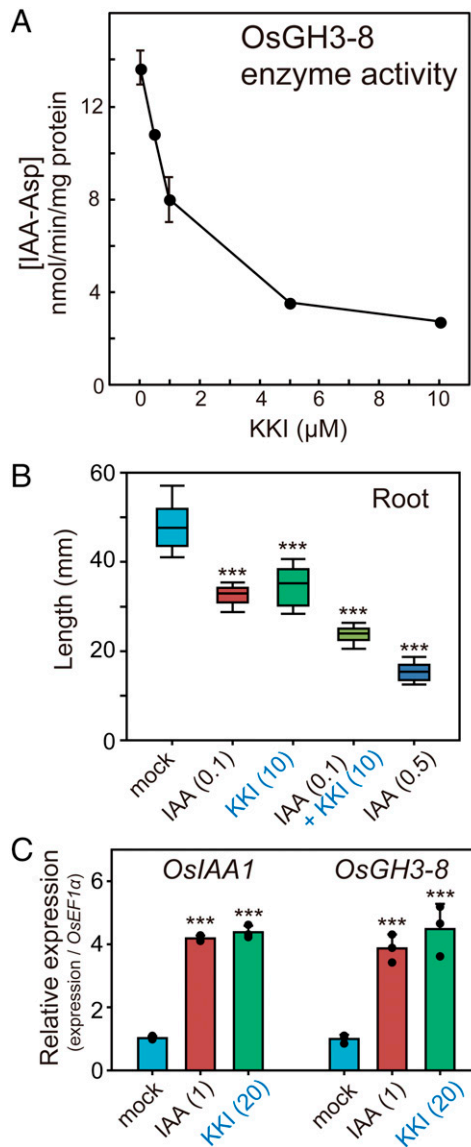
Fig. 5. KKI showed auxin-like activity in rice by inhibition of auxin-inactivating GH3 enzymes. (*A*) Inhibitory activity of KKI on recombinant OsGH3-8 enzyme. (*B*) Effects of KKI on primary root growth in rice. Two-day-old seedlings were incubated on 0.6% agar of sterile water containing indicated chemicals for 3 d. The root lengths were measured (*n* = 11). (*C*) Effects of KKI on auxin-inducible gene expression in rice root. Relative gene expression levels were quantified with qRT-PCR (*n* = 3). All data were standardized according to the expression levels of *OsEF1α*. Four-day-old seedlings were treated with the KKI or IAA for 30 min. (*B* and *C*) The values in parentheses represents the concentration of chemicals (micromolar). Error bars are SD. Asterisks indicate a statistically significant difference relative to mock treatment (***P < 0.001, Tukey's HSD test, *n* = 3).

ternary [ESI] complex. This inhibitory mechanism of KKI is consistent with the proposed kinetic mechanism (i.e., bi uni uni bi ping pong) of the GH3 proteins (42). Genetic approaches using *gh3* multiple mutants generated by CRISPR-Cas9 gene editing revealed that AtGH3.5, AtGH3.6, and AtGH3.17 predominantly function in IAA conjugation in the vegetative stage and that AtGH3.17 plays a fundamental role in basal IAA inactivation. In contrast, AtGH3.9 is critical for *Arabidopsis* fertility (23, 24). KKI showed the highest affinity for AtGH3.17 (K_i^{IAA} = 0.34 nM), although nanomolar affinities were measured for all the IAA-conjugating enzymes AtGH3.3, AtGH3.5, and AtGH3.6 (Fig. 3).

We also demonstrate the potential of KKI to dissect the role of the GH3 pathway in controlling auxin homeostasis. Cellular

IAA levels are coordinately modulated by the feedback regulation of IAA biosynthesis, inactivation, and transport (44). The *gh3-oct null* mutants maintain a high level of IAA throughout plant development (23). Accordingly, *gh3* multiple mutants have decreased IAA biosynthesis and enhanced IAA efflux as a consequence of such high levels of endogenous IAA. Conditional overexpression and knock-down systems generally take a few hours before the modulation of target protein function. Therefore, the kinetics of auxin homeostasis could not be effectively assessed by molecular genetic methods. On the other hand, KKI can rapidly knock down auxin inactivation mediated by GH3s. Consistent with the rapid degradation of DII-VENUS reporter protein and qRT-PCR analysis of auxin-inducible gene transcription (Fig. 4), our LC-MS/MS measurement demonstrated that the IAA level doubled 10 min after KKI treatment and that the IAA level continued to increase. This result implies that IAA is turned over within 10 min under steady-state homeostasis in WT plants (45). A previous study indicated that YUC inhibitor yucasin treatment decreased the endogenous IAA to almost basal level in maize coleoptile tips and *35S:YUC1* shoots within 30 min (46), supporting the hypothesis that IAA is rapidly inactivated *in planta*. Our results are the clearest indication yet that most endogenous IAA *in planta* would be turned over within 10 min and that this inactivation plays a pivotal role in IAA homeostasis. Many computational models of the auxin system assume parameters for synthesis, transport, and inactivation (47, 48). The inactivation rates of IAA in specific tissues and cells need to be considered in IAA distribution models together with IAA biosynthesis and polar transport. Recently, AuxSen, a new fluorescence resonance energy transfer–based biosensor for IAA visualization, was generated (49). By combining such genetic and metabolic tools, KKI will help provide greater insight into the dynamics of IAA homeostasis.

GH3 genes are widely conserved in diverse land plants and function as primary regulators in auxin homeostasis. Consistent with this, KKI caused typical high-auxin phenotypes such as primary root inhibition, much root hair, and increased lateral root formation in diverse vascular plants. In the moss *P. patens*, KKI induced the ectopic formation of leafy-like primordia in the gametophore. In *P. patens*, two *PpGH3* genes and two auxin efflux transport facilitators *PpPIN* genes have been functionally identified (50, 51), and the auxin efflux transport inhibitor NPA was shown to induce similar impaired phenotypes in the gametophore (50). This evidence implied that auxin transport and inactivation coordinately regulate the moss gametophore development. Overall, our study demonstrates that the GH3 inhibitor KKI will be a powerful tool to dissect auxin homeostasis in diverse land plants.

Materials and Methods

Plant Material and Growth Conditions. *Arabidopsis thaliana* accession Col-0 was used as WT. Transgenic seeds of *DR5::GUS* (33), *35S::YUC1* (52), *pMDC7::AtDAO1*, *pMDC7::IAMT1* (5, 14), *pMDC7::GH3.6* (53), *pMDC7::UGT84B1* (11), *35S::DII-VENUS* (44), *35S::JAZ1-GUS* (54), and *pJAZ2::GUS* lines (55) were previously described. The *axr1-3* (56) and *sav3-2* (36) single mutants, the *tir1-1 afb2-1* double mutant (34), *gh3-1 2 3 4 5 6 17 9*($^{+/-}$) septuple mutant (23), and the *yucQ* (*yucca3 5 7 8 9*) quintuple mutant (37) were previously reported. *Arabidopsis* seeds were sterilized and placed on GM media (1/2 Murashige and Skoog medium containing 1.2% [wt/vol] sucrose, 0.5 g/L Mes, B5 vitamins, and either 0.4% [for horizontal culture] or 1.4% [for vertical culture] of agar, pH 5.7 to 5.8). Seeds were stratified at 4 °C for 1 d and grown at 23 °C under continuous light (60 to 75 μmol·m^{-2}·s^{-1}; 380 to 780 nm) in a growth chamber (MLR-352; Panasonic). Plants on soil were grown in a cultivation room at 23 °C with continuous light (100 μmol·m^{-2}·s^{-1}).
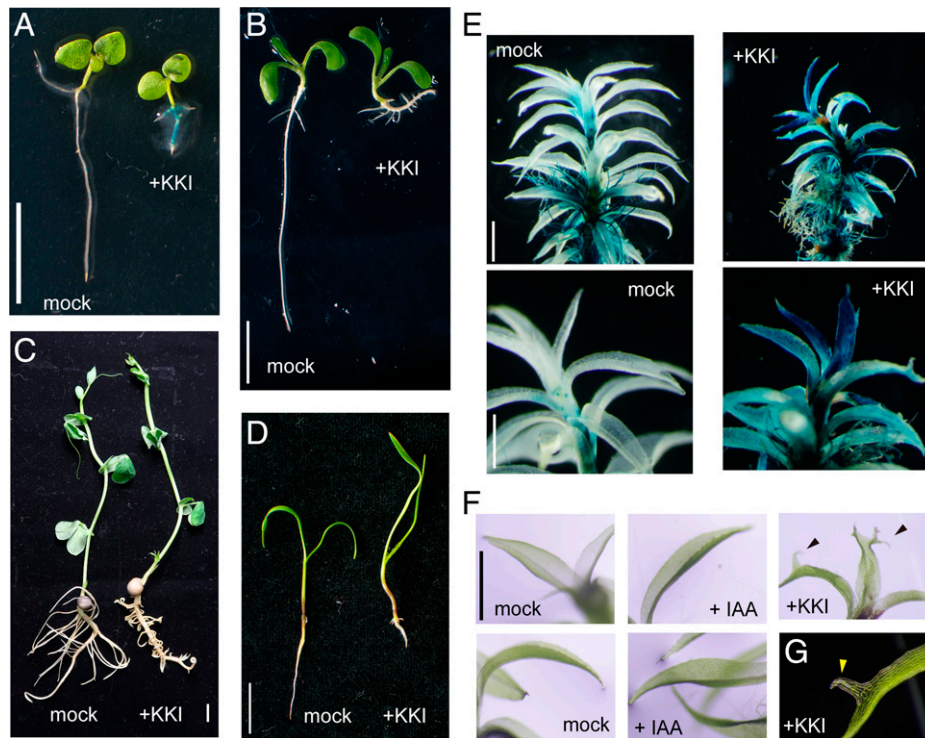
Fig. 6. KKI caused high-auxin phenotypes in various plants. (*A*) The *PS-IAA4/5::GUS* auxin-responsive tobacco reporter lines grown with 10 μM KKI on MS medium for 10 d. GUS expression was histochemically visualized with X-Gluc. (*B*) Lettuce seedlings were grown with 10 μM KKI on ½ MS medium for 12 d. (*C*) Mung bean (5-d-old) was placed on ½ MS medium containing 20 μM KKI and then cultured for another 9 d. (*D* and *F*) Carrot seedlings were grown on ½ MS medium with 10 μM KKI for 14 d. (*E–G*) The *GH3::GUS* auxin-responsive *P. patens* reporter lines grown with or without 10 μM KKI and 10 μM IAA on BCDATG medium for 15 d. (*E*) GUS expression was histochemically visualized with X-Gluc. (*F* and *G*) Arrows indicate the ectopic formation of leafy-like primordia. (Scale bars: 10 mm in *A–D*, 1 mm in *F*, and 0.25 mm in *G*).

Rice (*Oryza sativa* cv. Nipponbare) seeds were sterilized by 6% of sodium hypochlorite for 20 min, and then the seeds were washed with sterile water five times. For the mesocotyl assay, seeds were incubated in sterile distilled water at 28 °C for 2 d in dark conditions. The seedlings were submerged in sterile water containing indicated chemicals for 5 d (25 °C, 18 h light/6 h dark) and the mesocotyl length was measured. For the primary root assay, seeds were incubated in sterile water at 28 °C for 2 d in dark condition. The seedlings were cultured in sterile water (solidified with 0.6% agar) containing indicated chemicals for 5 d (25 °C, 18 h light/6 h dark) and the root length was measured.

Transgenic tobacco harboring the auxin-responsible *PS-IAA4/5::GUS* reporter gene (57) was grown on MS medium (0.3% agar) containing KKI for 10 d. GUS expression was histochemically visualized with X-Gluc (58). *L. sativa* (lettuce) seedlings were grown with KKI on 1/2 MS medium (0.3% agar) for 12 d. *D. carota* (carrot) seedlings were grown on 1/2 MS medium with KKI for 14 d. *V. radiata* (mung bean) was cultured on 1/2 MS medium for 5 d and then cultured for another 9 d on 1/2 MS medium containing KKI. The colony of *P. patens* auxin-responsible *GH3::GUS* reporter lines were cultured with or without KKI and IAA on BCDATG medium (0.8% agar) for 15 d (50). GUS expression was histochemically visualized with X-Gluc.

IAA Measurements. IAA metabolites were measured by the methods according to previously described (5); 30 to 40 mg of frozen plant tissues were added to the extract solution ($CH_3CN:H_2O = 8:2$, 1% AcOH) and homogenized with zirconia beads (φ = 3 mm) in a 2-mL microcentrifuge tube by using a Beads Crusher μT-12 (TAITEC) for 2 min. The phenyl-$^{13}C_6$IAA was used as the internal standard. The homogenates were purified with Oasis HLB column and Oasis WAX column (1 mL; Waters) as previously described. The IAA in purified fractions was analyzed with an Agilent 6420 Triple Quad system (Agilent Technologies) with a ZORBAX Eclipse XDB-C18 column (1.8 mm, 2.1 mm × 50 mm; Agilent Technologies).

Measurements of Primary and Lateral Root Growth. For primary root growth assays, *Arabidopsis* seedlings were vertically grown on GM plates containing KKI for 6 to 8 d under continuous light at 24 °C. Estradiol was added to

a medium (5 μM) to induce transgene in estradiol-inducible pMDC7 transgenic line. Primary root length was recorded by a digital camera. For lateral root assays, *Arabidopsis* seedlings were vertically grown for 6 d and then transferred to a horizontal GM plate (2 g/L gellan gum) containing chemicals. The seedlings were incubated for another 2 d at 24 °C. The number of lateral roots and primary root length were measured. The image was analyzed by NIH ImageJ software.

Recombinant Protein Expression. Full-length complementary DNA (cDNA) clones of *AtGH3.3*, *AtGH3.5*, *AtGH3.6*, *AtGH3.15*, and *AtGH3.17* were obtained from RIKEN Bioresource Center. Full-length open reading frame (ORF) were amplified by PrimeSTAR Max DNA Polymerase (Takara Bio) with each primer set and cloned into the BamHI and Hind III sites of the pCold I vector by In-Fusion Cloning (Takara Bio). The *OsGH3-8* ORF was synthesized according to the protein sequence of OsGH3-8 in the NCBI database (XP_015647797) and cloned into pCold I vector. For protein expression, *Escherichia coli* BL21 (DE3) carrying each respective expression construct was cultured in Terrific Broth medium (50 μg/mL ampicillin) at 37 °C until A$_{600}$ reached 0.5. Protein expression was induced by cold shock in cooled water (4 to 10 °C) for 30 min. Then, isopropyl-β-D-thiogalactoside was added (0.5 mM) and cultures were grown for 24 h at 15 °C. The cultured cells were collected by centrifugation (8,000 × *g* for 10 min at 4 °C) and suspended in BugBuster Protein Extraction Reagent according to the manufacturer's procedures (Merck Millipore). The supernatant was collected by centrifugation (12,000 × *g* for 10 min at 4 °C) and then applied to TALON metal affinity resin (Clontech). The column was washed with buffer I (0.5 M NaCl and 50 mM Tris·HCl buffer [pH 8.0]) and then buffer II (0.5 M NaCl, 50 mM Tris·HCl buffer [pH 8.0], and 5 mM imidazole). The purified protein was eluted with buffer III (0.5 M NaCl, 50 mM Tris·HCl buffer [pH 8.0], and 200 mM imidazole) and desalted by Spectra/Por Dialysis Membrane 3 (Spectrum Labs) with buffer IV (10 mM NaCl and 10 mM Tris·HCl buffer [pH 8.0]). The protein solution was added to 20% glycerol and stored at –80 °C until use.

Measurement for GH3 Enzyme Activity. GH3 enzyme assays are performed as previously described (22, 32). Briefly, the reaction mixture contained 50 mM Tris·HCl buffer (pH 8.6), 1 mM dithiothreitol, 3 mM MgCl$_2$, and recombinant

enzymes (AtGH3.3: 1.6 µg, AtGH3.5: 0.3 µg, AtGH3.6: 0.15 µg, AtGH3.15: 2.2 µg, AtGH3.17: 0.5 µg, and OsGH3.8: 1.1 µg) with varied concentrations of substrates (9 to 1,000 µM IAA, 3 to 3,000 µM ATP, and 50 to 3,000 µM amino acid) in a final volume of 100 µL. The enzyme reaction was carried out at 30 °C for 30 min. Then, 80 µL of the reaction mixture was added to 320 µL of methanol containing 50 mM phosphoric acid in a 1.5-mL microtube to terminate the reaction. After centrifugation at $12,000 \times g$ for 10 min at 4 °C, the 200 µL of supernatant was added to the 200 µL of MeOH:H₂O (1:4) solution and immediately analyzed by high-performance liquid chromatography (HPLC) (Extrema; Jasco). For the kinetic assays, the different concentrations of the substrates and KKI were added to the reaction mixtures.

In HPLC analysis, IAA, IAA-Asp, IAA-Glu, and IBA-Gln were detected by a fluorescent detector (λ_{ex} = 280 nm; λ_{em} = 360 nm) and ultraviolet absorption detector (λ = 254 nm). IAA, IAA-Asp, and IAA-Glu were analyzed by an Inertsil ODS-3 column (150 × 4.6 mm inside diameter) with 0.5 mL/min flow rate of the mobile phase (MeOH:H₂O = 43:57 containing 10 mM H₃PO₄). IBA-Gln was eluted with the mobile phase (MeOH:H₂O = 50:50 containing 20 mM H₃PO₄). The enzyme kinetics and the inhibitory mode of KKI were analyzed with Sigma plot 14 software.

DII-VENUS Reporter Assay. *DII-VENUS* seedlings (6-d-old) grown on vertical GM plates were used for the assay. The seedlings were treated with 2 µM FM4-64 dye for 10 min and then transferred to the GM plate containing IAA or KKI on the slide glass. The fluorescent image was recorded at regular intervals with FV-3000 laser scanning confocal microscope (Olympus) at regular intervals. The fluorescent intensity of NLS-localized VNENUS protein was analyzed with ImageJ software.

qRT-PCR. Five-day-old *Arabidopsis* seedlings grown on vertical GM plates were transferred to liquid GM medium and incubated for another 24 h. The seedlings were harvested at regular intervals after the addition of IAA and KKI to the medium. Four-day-old rice seedlings were incubated with a distilled water containing IAA or KKI for 30 min, and the excised roots were harvested. The samples were stored at –80 °C until RNA extraction. Total RNA was extracted from plant samples using NucleoSpin RNA Plant (Macherey Nagel GmbH & Co. KG) and used for first-strand cDNA synthesis by the ReverTra Ace qRT PCR Master mix (Toyobo). qRT-PCR was performed on StepOne Realtime PCR system (Applied Biosystems) using KAPA SYBR FAST qPCR Kits (Roche) and the gene-specific primer sets shown in SI Appendix, Table S1. The PCR program consisted of an initial temperature of 95 °C for 20 s, followed by 40 cycles of 95 °C for 3 s, 60 °C for 30 s. The expression levels of each gene were calculated by $\Delta\Delta$Ct method and normalized by the expression levels of reference genes (*AtUBQ10* for *Arabidopsis* and *OsEF1α* for rice).

SPR ASSAY of KKI Binding to Auxin Receptors. Assays of KKI binding to AtTIR1 and AtAFB5 were run according to the method of Quareshy et al. (38) using a Biacore T200.

Jasmonate-Responsive GUS Reporter Gene Assay. *Arabidopsis 35S::JAZ1-GUS* line and *pJAZ2::GUS* line were grown for 7 d (29). For the *35S::JAZ1-GUS* line (54), 7-d-old seedlings were cultured in liquid GM media with 20 µM of KKI for 30 min. JA and JA-Ile were added to the culture media and then incubated for another 30 min. For *pJAZ2::GUS* lines (55), 7-d-old seedlings were incubated

with 20 µM of KKI, JA, and JA-Ile for 6 h. The seedlings were stained with X-Glc and incubated at 37 °C until sufficient staining developed (58).

Synthesis of Chemicals. ¹H and ¹³C-NMR spectra were recorded on ECS400 and ECZ400 spectrometers (JEOL). Mass spectra were measured on autoflex speed MALDI-TOF MS (Bruker). KKI was synthesized according to previous reports (5) and is commercially available as a reagent (BioAcademia, catalog number 30-005).

For lead compound **1** (Fig. 1), to the solution of *N*-phthaloylglycine (207 mg, 1.0 mmol) in 4 mL of DMF was added 1-hydroxybenzotriazole monohydrate (134 mg, 1.0 mmol), *m*-anisidine (137 mg, 1.1 mmol), and WSCD-HCl (204 mg, 1.1 mmol). The reaction mixture was stirred at room temperature for 6 h. The reaction mixture was poured into water (10 mL) and extracted with EtOAc (20 mL two times) at pH 2 to 3. The EtOAc layer was washed with 1 M aqueous Na₂CO₃ solution (10 mL). The EtOAc layer was dried over anhydrous Na₂SO₄ and then concentrated *in vacuo*. The resulting powder was recrystallized from *n*-hexane–EtOAc. The lead compound **1** was obtained as a colorless powder (179 mg, 52% yield). m.p. = 180 to 187 °C; ¹H-NMR (400 MHz, CDCl₃) δ 7.88 (dd, J = 5.5, 3.2 Hz, 2H), 7.74 (dd, J = 5.5, 3.2 Hz, 2H), 7.26 (d, J = 4.1 Hz, 1H), 7.15 (t, J = 8.0 Hz, 1H), 6.92 (d, J = 9.2 Hz, 1H), 6.63 (d, J = 8.2 Hz, 1H), 4.50 (s, 2H), 3.74 (s, 3H); ¹³C-NMR (100 MHz, CDCl₃) δ 167.9, 164.3, 160.0, 138.4, 134.3, 131.9, 129.6, 123.7, 111.9, 110.8, 105.3, 55.2, 41.5; matrix-assisted laser desorption ionization–time of flight mass spectrometry [M+Na]⁺ *m/z* 333.1.

Statistical Analyses. All box plots and bar graphs were generated by Sigmaplot14 software. Statistical analysis was performed by one-way ANOVA Tukey's post hoc test and two-tailed *t* test. Box-and-whisker plots show a median (centerline), upper/lower quartiles (box limits), and maximum/minimum. For LC-MS/MS analysis, three biological replicates in an independent experiment were analyzed and the means of the replicates were indicated.

Data Availability. All study data are included in the article and/or *SI Appendix*.

Author affiliations: ªDepartment of Bioscience, Okayama University of Science, Okayama 700-0005, Japan; ᵇDepartment of Biochemistry, Okayama University of Science, Okayama 700-0005, Japan; ᶜDepartment of Biological Production Science, United Graduate School of Agricultural Science, Tokyo University of Agriculture and Technology, Fuchu 183-8509, Japan; ᵈDepartment of Biology, Washington University in St. Louis, St. Louis, MO 63130; ᵉSchool of Life Sciences, University of Warwick, Coventry CV4 7AS, United Kingdom; ᶠSection of Cell and Developmental Biology, University of California San Diego, La Jolla, CA 92093; ᵍGraduate School of Agriculture, Tokyo University of Agriculture and Technology, Fuchu 183-8509, Japan; and ʰRIKEN Center for Sustainable Resource Science, Kanagawa 230-0045, Japan

1. R. Casanova-Sáez, E. Mateo-Bonmatí, K. Ljung, Auxin metabolism in plants. *Cold Spring Harb. Perspect. Biol.* **13**, a039867 (2021).
2. H. Kasahara, Current aspects of auxin biosynthesis in plants. *Biosci. Biotechnol. Biochem.* **80**, 34–42 (2016).
3. M. Adamowski, J. Friml, PIN-dependent auxin transport: Action, regulation, and evolution. *Plant Cell* **27**, 20–32 (2015).
4. K. Mashiguchi et al., The main auxin biosynthesis pathway in Arabidopsis. *Proc. Natl. Acad. Sci. U.S.A.* **108**, 18512–18517 (2011).
5. K. I. Hayashi et al., The main oxidative inactivation pathway of the plant hormone auxin. *Nat. Commun.* **12**, 6752 (2021).
6. K. Müller et al., Dioxygenase for auxin oxidation 1 catalyzes the oxidation of IAA amino acid conjugates. *Plant Physiol.* **187**, 103–115 (2021).
7. P. E. Staswick et al., Characterization of an Arabidopsis enzyme family that conjugates amino acids to indole-3-acetic acid. *Plant Cell* **17**, 616–627 (2005).
8. S. Porco et al., Dioxygenase-encoding AtDAO1 gene controls IAA oxidation and homeostasis in Arabidopsis. *Proc. Natl. Acad. Sci. U.S.A.* **113**, 11016–11021 (2016).
9. J. Zhang et al., DAO1 catalyzes temporal and tissue-specific oxidative inactivation of auxin in Arabidopsis thaliana. *Proc. Natl. Acad. Sci. U.S.A.* **113**, 11010–11015 (2016).
10. R. G. Jackson et al., Over-expression of an Arabidopsis gene encoding a glucosyltransferase of indole-3-acetic acid: Phenotypic characterisation of transgenic lines. *Plant J.* **32**, 573–583 (2002).
11. Y. Aoi et al., UDP-glucosyltransferase UGT84B1 regulates the levels of indole-3-acetic acid and phenylacetic acid in Arabidopsis. *Biochem. Biophys. Res. Commun.* **532**, 244–250 (2020).
12. G. Qin et al., An indole-3-acetic acid carboxyl methyltransferase regulates Arabidopsis leaf development. *Plant Cell* **17**, 2693–2704 (2005).
13. M. Abbas et al., Auxin methylation is required for differential growth in *Arabidopsis*. *Proc. Natl. Acad. Sci. U.S.A.* **115**, 6864–6869 (2018).
14. E. Takubo et al., Role of Arabidopsis indole-3-acetic acid carboxyl methyltransferase 1 in auxin metabolism. *Biochem. Biophys. Res. Commun.* **527**, 1033–1038 (2020).
15. J. M. Jez, Connecting primary and specialized metabolism: Amino acid conjugation of phytohormones by gretchen hagen 3 (GH3) acyl acid amido synthetases. *Curr. Opin. Plant Biol.* **66**, 102194 (2022).
16. P. E. Staswick, I. Tiryaki, M. L. Rowe, Jasmonate response locus JAR1 and several related Arabidopsis genes encode enzymes of the firefly luciferase superfamily that show activity on jasmonic, salicylic, and indole-3-acetic acids in an assay for adenylation. *Plant Cell* **14**, 1405–1415 (2002).

17. C. S. Westfall et al., Structural basis for prereceptor modulation of plant hormones by GH3 proteins. Science 336, 1708–1711 (2012).
18. C. K. Holland et al., Brassicaceae-specific gretchen hagen 3 acyl acid amido synthetases conjugate amino acids to chorismate, a precursor of aromatic amino acids and salicylic acid. J. Biol. Chem. 294, 16855–16864 (2019).
19. D. A. Korasick, T. A. Enders, L. C. Strader, Auxin biosynthesis and storage forms. J. Exp. Bot. 64, 2541–2555 (2013).
20. J. Ludwig-Müller, Auxin conjugates: Their role for plant development and in the evolution of land plants. J. Exp. Bot. 62, 1757–1773 (2011).
21. S. Sugawara et al., Distinct characteristics of indole-3-acetic acid and phenylacetic acid, two common auxins in plants. Plant Cell Physiol. 56, 1641–1654 (2015).
22. A. M. Sherp, C. S. Westfall, S. Alvarez, J. M. Jez, Arabidopsis thaliana GH3.15 acyl acid amido synthetase has a highly specific substrate preference for the auxin precursor indole-3-butyric acid. J. Biol. Chem. 293, 4277–4288 (2018).
23. R. Guo et al., Local conjugation of auxin by the GH3 amido synthetases is required for normal development of roots and flowers in Arabidopsis. Biochem. Biophys. Res. Commun. 589, 16–22 (2022).
24. R. Casanova-Sáez et al., Inactivation of the entire Arabidopsis group II GH3s confers tolerance to salinity and water deficit. New Phytol. 235, 263–275 (2022).
25. Z. Zheng et al., Local auxin metabolism regulates environment-induced hypocotyl elongation. Nat. Plants 2, 16025 (2016).
26. K. I. Hayashi, Chemical biology in auxin research. Cold Spring Harb. Perspect. Biol. 13, a040105 (2021).
27. S. Tsugafune et al., Yucasin DF, a potent and persistent inhibitor of auxin biosynthesis in plants. Sci. Rep. 7, 13992 (2017).
28. C. Böttcher et al., A novel tool for studying auxin-metabolism: The inhibition of grapevine indole-3-acetic acid-amido synthetases by a reaction intermediate analogue. PLoS One 7, e37632 (2012).
29. C. Meesters et al., A chemical inhibitor of jasmonate signaling targets JAR1 in Arabidopsis thaliana. Nat. Chem. Biol. 10, 830–836 (2014).
30. R. A. Okrent, M. C. Wildermuth, Evolutionary history of the GH3 family of acyl adenylases in rosids. Plant Mol. Biol. 76, 489–505 (2011).
31. C. S. Westfall et al., Arabidopsis thaliana GH3.5 acyl acid amido synthetase mediates metabolic crosstalk in auxin and salicylic acid homeostasis. Proc. Natl. Acad. Sci. U.S.A. 113, 13917–13922 (2016).
32. T. Ulmasov, J. Murfett, G. Hagen, T. J. Guilfoyle, Aux/IAA proteins repress expression of reporter genes containing natural and highly active synthetic auxin response elements. Plant Cell 9, 1963–1971 (1997).
33. G. Parry et al., Complex regulation of the TIR1/AFB family of auxin receptors. Proc. Natl. Acad. Sci. U.S.A. 106, 22540–22545 (2009).
34. N. Dharmasiri et al., AXL and AXR1 have redundant functions in RUB conjugation and growth and development in Arabidopsis. Plant J. 52, 114–123 (2007).
35. Y. Tao et al., Rapid synthesis of auxin via a new tryptophan-dependent pathway is required for shade avoidance in plants. Cell 133, 164–176 (2008).
36. Q. Chen et al., Auxin overproduction in shoots cannot rescue auxin deficiencies in Arabidopsis roots. Plant Cell Physiol. 55, 1072–1079 (2014).
37. M. Quareshy, V. Uzunova, J. M. Prusinska, R. M. Napier, Assaying auxin receptor activity using SPR assays with F-box proteins and Aux/IAA degrons. Methods Mol. Biol. 1497, 159–191 (2017).
38. W. Teale, K. Palme, Naphthylphthalamic acid and the mechanism of polar auxin transport. J. Exp. Bot. 69, 303–312 (2018).
39. I. Casimiro et al., Auxin transport promotes Arabidopsis lateral root initiation. Plant Cell 13, 843–852 (2001).
40. X. Shan, Y. Zhang, W. Peng, Z. Wang, D. Xie, Molecular mechanism for jasmonate-induction of anthocyanin accumulation in Arabidopsis. J. Exp. Bot. 60, 3849–3860 (2009).
41. Q. Chen, C. S. Westfall, L. M. Hicks, S. Wang, J. M. Jez, Kinetic basis for the conjugation of auxin by a GH3 family indole-acetic acid-amido synthetase. J. Biol. Chem. 285, 29780–29786 (2010).
42. G. Xu et al., Crystal structure of the acyl acid amido synthetase GH3-8 from Oryza sativa. Biochem. Biophys. Res. Commun. 534, 266–271 (2021).
43. G. Brunoud et al., A novel sensor to map auxin response and distribution at high spatio-temporal resolution. Nature 482, 103–106 (2012).
44. S. Takato et al., Auxin signaling through SCF$^{TIR1/AFBs}$ mediates feedback regulation of IAA biosynthesis. Biosci. Biotechnol. Biochem. 81, 1320–1326 (2017).
45. E. M. Kramer, E. M. Ackelsberg, Auxin metabolism rates and implications for plant development. Front Plant Sci 6, 150 (2015).
46. T. Nishimura et al., Yucasin is a potent inhibitor of YUCCA, a key enzyme in auxin biosynthesis. Plant J. 77, 352–366 (2014).
47. M. Cieslak, A. Owens, P. Prusinkiewicz, Computational models of auxin-driven patterning in shoots. Cold Spring Harb. Perspect. Biol. 14, a040097 (2022).
48. A. Morales-Tapia, A. Cruz-Ramírez, Computational modeling of auxin: A foundation for plant engineering. Front Plant Sci 7, 1881 (2016).
49. O. Herud-Sikimić et al., A biosensor for the direct visualization of auxin. Nature 592, 768–772 (2021).
50. T. A. Bennett et al., Plasma membrane-targeted PIN proteins drive shoot development in a moss. Curr. Biol. 24, 2776–2785 (2014).
51. J. Ludwig-Müller, S. Jülke, N. M. Bierfreund, E. L. Decker, R. Reski, Moss (Physcomitrella patens) GH3 proteins act in auxin homeostasis. New Phytol. 181, 323–338 (2009).
52. C. Won et al., Conversion of tryptophan to indole-3-acetic acid by tryptophan aminotransferases of Arabidopsis and YUCCAs in Arabidopsis. Proc. Natl. Acad. Sci. U.S.A. 108, 18518–18523 (2011).
53. K. Tanaka et al., UGT74D1 catalyzes the glucosylation of 2-oxindole-3-acetic acid in the auxin metabolic pathway in Arabidopsis. Plant Cell Physiol. 55, 218–228 (2014).
54. D. Tripathi, T. Zhang, A. J. Koo, G. Stacey, K. Tanaka, Extracellular ATP acts on jasmonate signaling to reinforce plant defense. Plant Physiol. 176, 511–523 (2018).
55. P. Figueroa, J. Browse, The Arabidopsis JAZ2 promoter contains a G-Box and thymidine-rich module that are necessary and sufficient for jasmonate-dependent activation by MYC transcription factors and repression by JAZ proteins. Plant Cell Physiol. 53, 330–343 (2012).
56. C. Lincoln, J. H. Britton, M. Estelle, Growth and development of the axr1 mutants of Arabidopsis. Plant Cell 2, 1071–1080 (1990).
57. L. M. Wong et al., Differential activation of the primary auxin response genes, PS-IAA4/5 and PS-IAA6, during early plant development. Plant J. 9, 587–599 (1996).
58. A. Oochi et al., Pinstatic acid promotes auxin transport by inhibiting PIN internalization. Plant Physiol. 180, 1152–1165 (2019).